Developmental Biology 453 (2019) 130–140

Contents lists available at ScienceDirect

Developmental Biology

journal homepage: www.elsevier.com/locate/developmentalbiology

Multicolor lineage tracing using *in vivo* time-lapse imaging reveals coordinated death of clonally related cells in the developing vertebrate brain

Nicole L. Brockway [a,1], Zoe T. Cook [a,1], Maritte J. O'Gallagher [a,1], Zachary J.C. Tobias [a,1], Mako Gedi [a], Kristine M. Carey [a], Vivek K. Unni [b], Y. Albert Pan [c], Margaret R. Metz [a], Tamily A. Weissman [a,*]

[a] Department of Biology, Lewis & Clark College, Portland, OR, 97219, USA
[b] Department of Neurology, Oregon Health & Science University, Portland, OR, 97239, USA
[c] Developmental and Translational Neurobiology Center, Fralin Biomedical Research Institute at Virginia Tech Carilion, Virginia Tech, Roanoke, VA, 24016, USA

ARTICLE INFO

Keywords:
Zebrafish
Brainbow
In vivo imaging
Competition
Hindbrain
Development
Nervous system
Apoptosis
Zebrabow

ABSTRACT

The global mechanisms that regulate and potentially coordinate cell proliferation & death in developing neural regions are not well understood. In particular, it is not clear how or whether clonal relationships between neural progenitor cells and their progeny influence the growing brain. We have developed an approach using Brainbow in the developing zebrafish to visualize and follow multiple clones of related cells *in vivo* over time. This allows for clear visualization of many dividing clones of cells, deep in proliferating brain regions. As expected, in addition to undergoing interkinetic nuclear migration and cell division, cells also periodically undergo apoptosis. Interestingly, cell death occurs in a non-random manner: clonally related cells are more likely to die in a progressive fashion than cells from different clones. Multiple members of an individual clone die while neighboring clones appear healthy and continue to divide. Our results suggest that clonal relationships can influence cellular fitness and survival in the developing nervous system, perhaps through a competitive mechanism whereby clones of cells are competing with other clones. Clonal cell competition may help regulate neuronal proliferation in the vertebrate brain.

1. Introduction

In developing organs, specialized progenitor cells divide repeatedly during an early proliferative period to generate daughter cells that differentiate and populate the growing tissue (McConnell, 1995; Conlon and Raff, 1999). Tight regulation of this growth is particularly important in the nervous system, where the relative size of different brain regions and the complexity of neural circuitry can directly impact behavior (Caviness et al., 1995; Lui et al., 2011; Florio and Huttner, 2014; Homem et al., 2015). In the developing brain, neurons are produced by neural progenitor cells, including radial glia that divide in proliferative zones lining the cerebral ventricles (Malatesta et al., 2000; Noctor et al., 2001; Kriegstein and Alvarez-Buylla, 2009). The specific subset of progenitor cell types that are present in a given species and their pattern of cell division can ultimately determine brain structure (Lui et al., 2011; Nonaka-Kinoshita et al., 2013; Nomura et al., 2016; Namba and Huttner, 2017). While a number of regulatory factors and pathways have been identified that influence neuronal progenitor function (McConnell, 1995; Corbin et al., 2008; Lui et al., 2011; Namba and Huttner, 2017), the global mechanisms that regulate and stabilize overall brain size within a species are not fully understood. Proliferation may be coordinated with and balanced by programmed cell death during development (Raff, 1996; Miguel-Aliaga and Thor, 2009; Yamaguchi and Miura, 2015).

One potential regulatory mechanism for proliferation was identified in the *Drosophila* wing imaginal disc, and is known as clonal "cell competition" (Morata and Ripoll, 1975; Simpson, 1979; Simpson and Morata, 1981; Merino et al., 2016), whereby clones of dividing cells compete with one another. "Winner" clones survive while "loser" clones die by apoptosis. Cell competition in development has been demonstrated in a number of systems including vertebrates (Micklem et al.,

* Corresponding author. Lewis & Clark College, USA.
E-mail address: weissman@lclark.edu (T.A. Weissman).
[1] These authors contributed equally to this work.

https://doi.org/10.1016/j.ydbio.2019.05.006
Received 27 March 2019; Received in revised form 12 May 2019; Accepted 12 May 2019
Available online 16 May 2019

1972; Clavería et al., 2013; Sancho et al., 2013; Villa del Campo et al., 2014; Weissman, 2015; Walderich et al., 2016), and can be driven by intrinsic cell properties or by the availability of extracellular resources (Moreno et al., 2002; De La Cova et al., 2004; Moreno and Basler, 2004; Clavería et al., 2013; Levayer and Moreno, 2013; Sancho et al., 2013; Villa del Campo et al., 2014). *Drosophila* genes implicated in clonal cell competition are present in the vertebrate nervous system, raising the intriguing idea that competition among vertebrate neural progenitor clones could regulate growth in the developing brain. Competition at the level of whole clones of commonly derived cells represents a level of organization that has not been demonstrated in the vertebrate nervous system. In theory, neural progenitors along with their progeny would together compete against other such clones to determine which are most fit to survive. These interactions could ultimately determine the resulting number and make-up of neurons that will populate the mature brain. Identification of such a regulatory pathway could expand understanding of the mechanisms that control growth and size in nervous tissues.

If clones of dividing cells indeed compete with one another in the developing brain, one would expect to find evidence for winner clones that proliferate successfully, alongside loser clones that undergo coordinated apoptosis. Consistent with this possibility, compensatory proliferation of wild-type cells occurs following apoptosis of nearby abnormal cells expressing excessive centrioles in the developing neuroepithelium (Dzafic et al., 2015). Furthermore, TUNEL staining in fixed brain tissue has revealed small clusters of dying cells (Cole and Ross, 2001), although the approaches used did not address clonal identity.

To test whether clonal cell competition could help regulate neural development, a robust system is needed for following multiple distinct clones of related cells *in vivo*, which until recently has not been possible. Apoptosis has been observed within the developing brain (Oppenheim, 1991; Kuan et al., 2000); however, to date it has been difficult to study any potential underlying clonal relationships *among* dying cells. In part this is due to technical limitations that make it difficult to clearly distinguish among and visualize multiple clones of dividing cells. Furthermore, the mammalian brain (with proliferative regions often nestled along the inner-most ventricles) is particularly difficult to visualize *in vivo*. Although the dynamic nature of mammalian brain development has been elegantly explored in organotypic slice culture (Bolz et al., 1990; Chenn and McConnell, 1995; Haydar et al., 1999; Dammerman et al., 2000; Letinic and Rakic, 2001; Miyata et al., 2001; Noctor et al., 2001; Palmer et al., 2001; LoTurco et al., 2003; Yu et al., 2009; Hansen et al., 2010), this approach disrupts the brain's natural milieu, while studies done in fixed tissue cannot use a longitudinal approach.

We have developed a system that moves beyond these limitations, enabling us to follow multiple clones of dividing cells in real time in the brain of living zebrafish, a powerful *in vivo* model for vertebrate development (Ingham, 1997; Wullimann and Mueller, 2004; Howe et al., 2013). To identify and unambiguously track multiple dividing clones in neural proliferative zones, we have adapted the Brainbow multicolor labeling approach (Livet et al., 2007; Pan et al., 2011, 2013; Weissman and Pan, 2014; Cook et al., 2018). Using *in vivo* confocal time-lapse imaging in larval zebrafish, we visualize the real-time dynamics of multiple dividing cell populations, consisting of neural progenitors radially arrayed with their color-coded progeny. We demonstrate *in vivo* that proliferating cells indeed undergo apoptosis during normal development *in a non-random manner*. Specifically, multiple members of one clone, and occasionally whole clones (dividing neuronal progenitor cells along with their progeny) can undergo coordinated apoptosis ("clonal apoptosis"), while neighboring clones appear normal. Clonal apoptosis often begins in one daughter cell, within hours following mitosis. The remaining clone members apoptose in a progressive manner within several hours following the first clone member's death. The overall frequency of apoptosis that we observe *in vivo* is similar to that measured in previous studies (Cole and Ross, 2001; Lyons et al., 2003; van Ham et al., 2010) and is not affected by the duration of the imaging. Taken together, our results demonstrate for the first time that clones of dividing neural progenitor cells and their progeny can undergo coordinated death during normal development. Our findings raise the possibility that clonal cell competition could be a critical regulator of growth in the vertebrate nervous system.

2. Materials & methods

2.1. Zebrafish care and transient brainbow expression

All protocols involving zebrafish were approved by the Lewis & Clark Institutional Animal Care and Use Committee. Adult wild-type zebrafish (*Danio rerio*; AB/TL; Westerfield, 2000; Zebrafish International Resource Center, Eugene, OR) were maintained in a controlled, multi-tank aquatic housing system (Aquaneering, Inc., San Diego, CA) at 27 °C in reverse osmosis (RO) water dosed for pH and salinity control. Injected embryos and larvae were maintained in an incubator (Forma Scientific, Marjetta, OH) at 28 °C in 90 mm Petri dishes (Genesee Scientific, San Diego, CA) containing E3 embryo medium (Nüsslein-Volhard et al., 2002; 5mM NaCl, J.T. Baker, Philipsburg, NJ; 0.17mM KCl, AMRESCO; 0.33mM CaCl2; 0.33mM MgSO4, Sigma, St. Louis, MO; and 0.00001% methylene blue, Sigma) with 0.2 mM phenylthiourea (PTU; Alfa Aesar, Ward Hill, MA) added at 1 day post-fertilization (dpf) to prevent pigmentation.

Hsp:Zebrabow plasmid DNA was generated by inserting the zebrafish *hsp70* promoter into the Zebrabow-GateDest destination vector (Pan et al., 2013) via single-site LR Gateway recombination (Invitrogen). Hsp:Zebrabow contains the Brainbow cassette from the CMV-Brainbow-1.0L plasmid (Livet et al., 2007), and contains dTomato as the default color, which can change upon Cre-mediated recombination to either monomeric Cerulean (referred to here as CFP) or EYFP (referred to here as YFP; see construct in Fig. 1A).

For transient expression via microinjection, brief pulses of air (World Precision Instruments, Sarasota, FL) were used to inject DNA solution from a glass capillary (World Precision Instruments; item TW100F-4) pulled on a micropipette puller (Sutter Instrument Company, Novato, CA) into the yolk of one-cell-stage wild-type AB/TL embryos within 45 min of fertilization. DNA solution contained ~10 ng/μL hsp:Zebrabow plasmid DNA, 3.75U Cre recombinase enzyme (New England Biolabs, Ipswich, MA; M0298M), and 2.5% phenol red in 0.1 mM KCl. Approximately 4.2 nL of this solution was injected into each embryo, equivalent to 42 pg plasmid DNA. To induce transgene expression via the heat-shock promoter, embryos underwent heat shock in a 50 mL tube submerged in a water bath at 37 °C for 80-90 min at 24 h post fertilization (hpf), coinciding with the known period of hindbrain neurogenesis (Trevarrow et al., 1990). Within 4 h, injected embryos were screened for Brainbow expression using an epifluorescence compound microscope (Zeiss) and embryos with robust fluorescent expression in yellow, cyan, and red channels were selected for imaging.

2.2. Imaging

All imaging was performed on a laser-scanning confocal microscope (Carl Zeiss LSM 710, Oberkochen, Germany). For Brainbow imaging, a DPSS 561 laser was used to excite dTomato, an Argon laser was used to excite CFP (mCerulean) at 458 nm, and YFP (EYFP) at 514 nm. For *in vivo* imaging, each fluorescent protein (FP) channel was imaged sequentially by line. Collection ranges for Brainbow were set to 463-509 nm for CFP, 519-555 nm for YFP, and 566-691 nm for dTomato. These settings differed for four-channel fixed imaging (see below). A transmitted light image was collected sequentially for some stacks. Images were acquired using Zen Black software (Carl Zeiss, Oberkochen, Germany), saved as .czi files, and subsequently imported into Fiji software (Schindelin et al., 2012) using the BioFormats Importer (The Open Microscopy Environment) and/or Imaris software (Bitplane, Zurich). For on-screen display, the dTomato channel was coded as red, the YFP channel was coded as green, and the CFP channel was coded as blue.

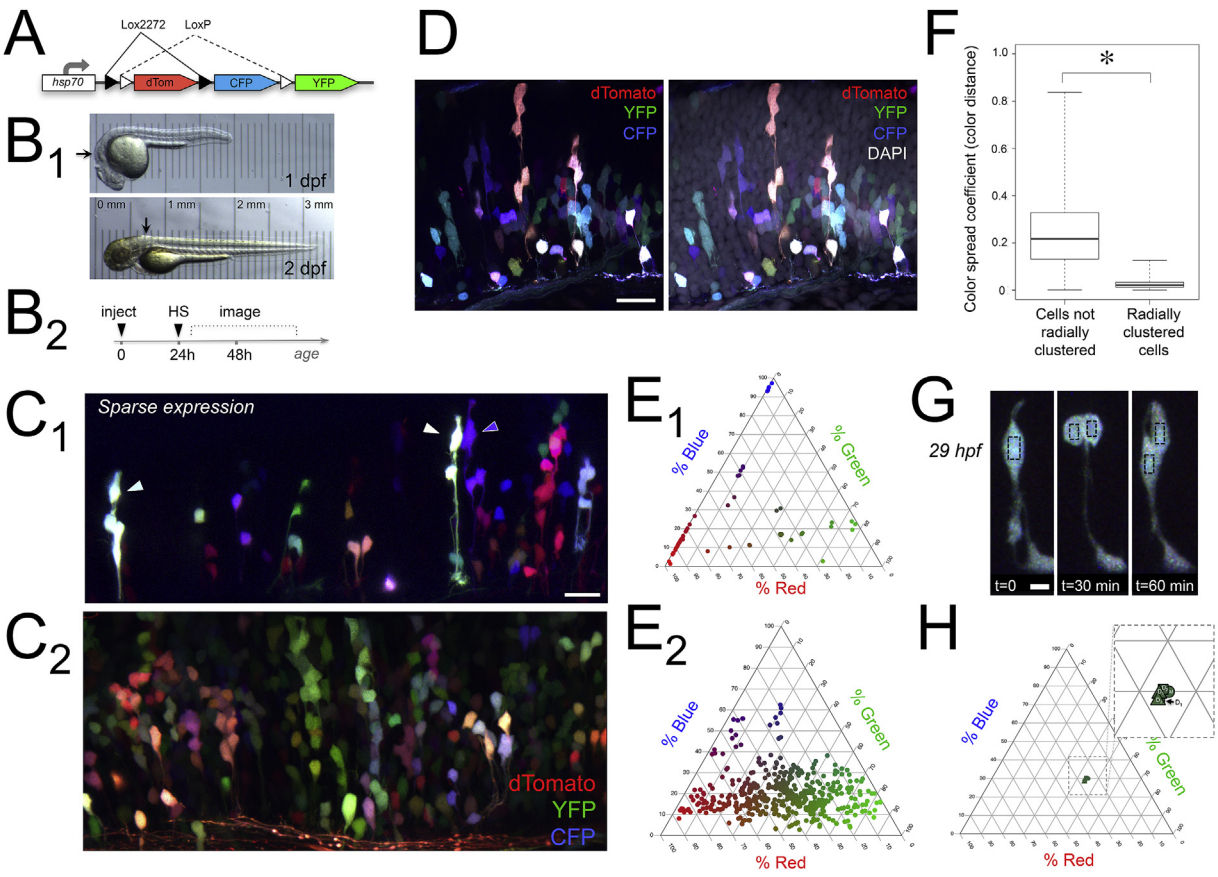

Fig. 1. Brainbow labels clonally related clusters of dividing cells in the developing zebrafish hindbrain.
A) Schematic of hsp:Zebrabow (Brainbow) DNA transiently expressed to color-code clones. B1) *In vivo* transmitted light images of developing zebrafish at 1 and 2 dpf; arrows indicate general hindbrain region targeted for imaging. Translucency of embryo is demonstrated by micrometer placed below each fish. B2) Experimental timeline showing injections at one-cell stage, heat shock (HS) at 24 h, and imaging from 1 to 3 dpf. C) *In vivo* Brainbow expression in the hindbrain, shown in maximum intensity projections representing 41μm in sparsely labeled 51 hpf zebrafish (C_1), and 81μm in 63.5 hpf zebrafish (C_2). In all panels, dorsal is up and rostral is to the left. D) DAPI staining of Brainbow-expressing zebrafish fixed at 51 hpf shows non-labeled cells for calculating labeling density; DAPI staining is coded as white for display (maximum intensity projection representing 3.4μm). E) Color of cells in C_1 and C_2 is quantified as relative channel weights in corresponding ternary plots (n=54 cells; 461 cells). F) Color spread coefficient, or distance between two colors, is significantly smaller between cells that are radially clustered. Coefficient values were obtained from pairwise comparisons between cells in hindbrain shown in C_2 (n=360 cells). Whiskers show extremes of data while an asterisk indicates a significant difference in color spread coefficient (Welch Two Sample *t*-test, t(648.66)=170.59, $p < 2.2 \times 10^{-16}$). G) Cell color remains relatively constant in daughter cells following cell division. Series of time points showing *in vivo* mitotic event in hindbrain of 29 hpf Brainbow-labeled zebrafish over 1 h (maximum intensity projections, 30μm depth). Color of mother and daughter cells, indicated by black boxes in G, is represented as relative channel weights in ternary plot in H; inset shows zoom of same plot to allow viewing of tightly clustered cell colors (M is mother; D1 and D2 are daughters at 30 min/squares, and 60 min/triangles). Scale bars represent 20μm in C_1, 16μm in C_2, 20μm in D, and 5μm in G. In C, D, and G, dTomato is coded as red, YFP is coded as green, and CFP is coded as blue.

2.3. In vivo imaging

For *in vivo* imaging experiments, zebrafish were anesthetized in approximately 0.2 mM MS-222 Tricaine-S (Western Chemical, Inc., Ferndale, WA) diluted in E3 medium, then placed in 60 mm Petri dishes, mounted for a dorsal or sagittal view on agarose pads (3%), and embedded in 1% low-melt agarose (Agarose SFR; AMRESCO, Solon, OH). For short interval time-lapses, fish remained on the microscope for the duration of the time observed. For 2 and 3 dpf time points in Fig. 2A only, fish were removed from the microscope, taken out of agarose and returned to Petri dishes at 28 °C in between time points. During this 24 h time period the brain tissue grows significantly and can lead to slight changes in cell position and depth. Images and movies of live-mount zebrafish were taken with a Zeiss 20x (1.0 NA) water immersion objective with zoom ranging from 1.0 to 2.5. For time-lapse imaging, the time interval between captured Z-stacks was 12, 30, or 32 min. Brightfield images in Fig. 1A were taken on a Zeiss Discovery V8 stereo microscope, with fish mounted in 3% methyl cellulose (Sigma, St. Louis).

Supplementary data related to this article can be found online at https://doi.org/10.1016/j.ydbio.2019.05.006

2.4. Fixed imaging

For fixed imaging experiments, whole-mount stained zebrafish were positioned onto glass slides in Vectashield mounting medium (Vector Laboratories, Burlingame, CA) and sealed under a glass coverslip supported by small drops of vacuum grease (Dow Corning, Midland, MI). Slides were stored in a dark chamber at 4 °C for up to 3 days prior to imaging. Whole-mount zebrafish were imaged with a Zeiss 40x (1.3 NA) oil immersion objective (zoom 1.3). A HeNe633 laser line was used to image AlexaFluor633. For fixed, four-channel imaging, YFP and Alexa633 were acquired simultaneously on one track, with dTomato and CFP acquired simultaneously on a second track. The two tracks were imaged sequentially by frame. Collection ranges were set to 463-509 nm for CFP, 519-570 nm for YFP, 566-691 nm for dTomato, and 638–747 for Alexa633. For DAPI imaging (used to measure labeling density), four-channel images were configured as dTomato and DAPI on one track, and YFP and CFP on a second track. Collection ranges were identical to above with DAPI collected between 410-430 nm.

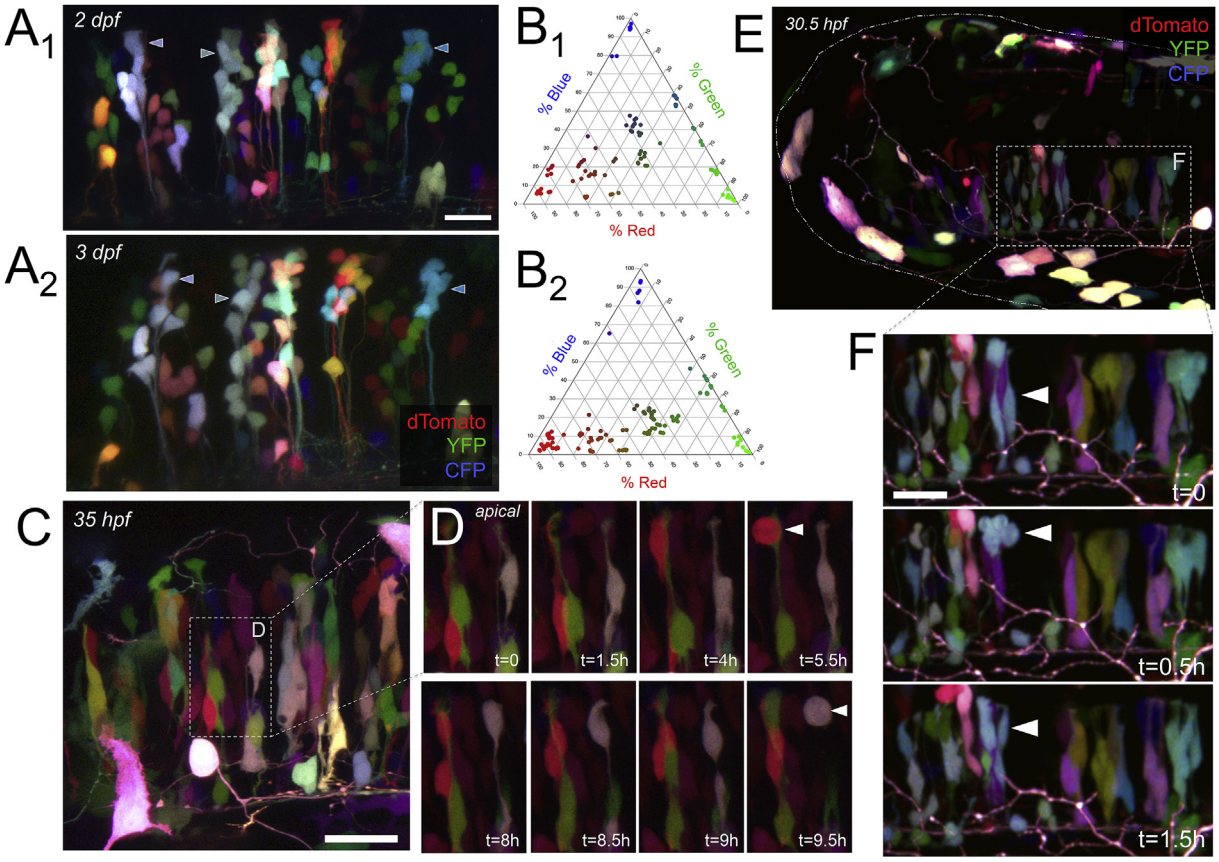

Fig. 2. Time-lapse *in vivo* imaging combined with Brainbow color-coding distinguishes multiple neighboring clones of cells undergoing interkinetic nuclear migration and dividing.

A) Color-coded radial clusters labeled in one fish expressing Brainbow at 2 dpf (55 hpf; A_1) and 3 dpf (71 hpf; A_2); maximum intensity projections representing 62μm and 47μm respectively. Three color-coded radial clusters are identified with arrowheads at each time point. The color of all Brainbow-labeled cells in A_1 and A_2 is quantified as relative channel weights in the corresponding ternary plots in B_1 and B_2 (n=106 cells, 119 cells). C) Zebrafish hindbrain at 35 hpf labeled with Brainbow (maximum intensity projection showing 24μm); inset indicated with dashed white box is the first time point displayed in D. D) Series of time points taken at 30 min intervals in the hindbrain from C. Over period of 9.5 h shown, labeled cells underwent interkinetic nuclear migration; white arrowheads indicate a cell at the apical surface. Rounding up of the cell soma at the apical surface and a corresponding increase in clone number (e.g., red cell at 5.5h and then 8h) was considered a mitotic event. E) Dorsolateral view of zebrafish hindbrain at 30.5 hpf labeled with Brainbow, where white dashed-and-dotted line shows approximate boundary of head, and white dashed box indicates inset shown in first time point of F. F) Series of time points taken at 30 min intervals in the hindbrain from E. Over a period of 1.5 h, two blue cells indicated by the white arrowheads can be observed moving to the apical surface and undergoing mitosis, suggesting a clone containing two progenitor cells. Scale bar represents 20μm in A, 25μm in C, and 20μm in F. In A through D, dorsal is up and rostral is to the left. In E and F, rostral is to the left. In all images, dTomato is coded as red, YFP is coded as green, and CFP is coded as blue.

2.5. Whole-mount immunohistochemistry

For whole-mount immunostaining, uninjected and Brainbow-injected fish at 1 and 2 dpf were fixed in 4% paraformaldehyde at 4 °C overnight, then dehydrated in 100% methanol at -20 °C for 15 min. Whole embryos were then rehydrated in 75%, 50%, and 25% methanol in phosphate-buffered saline (AMRESCO, Solon OH), 0.1% TritonX-100 (Sigma, St. Louis; PBST) for 5 min each, rinsed with PBST twice for 5 min, and then incubated in blocking solution (PBS 5% normal goat serum, 1% Triton X-100, 1% BSA, 1% DMSO; Sigma for each) for 1 h at room temperature (RT). After blocking, embryos were incubated overnight with anti-activated caspase3 primary antibody (BD Sciences, San Jose; 55956) diluted 1:200 in antibody buffer (20% block in PBST), then washed three times with PBST (20 min each). For secondary antibody staining, embryos were incubated with goat anti-rabbit IgG Alexa633 (Invitrogen, Carlsbad, CA, A21070) diluted 1:200 in antibody buffer overnight at RT, then washed three times with PBST and once with PBS (20 min each) before short-term storage in PBS at 4 °C. For DAPI staining, fixed embryos were incubated in 10mg/mL DAPI (Invitrogen, D1306) additionally diluted 1:10,000 in PBS for 2 h at RT, then washed twice with PBST (20 min each) and transferred to PBS for short-term storage at 4 °C. Uninjected fish were maintained in a manner identical to Brainbow-injected fish except that they did not undergo injection or heat shock.

2.6. Data analysis

2.6.1. 5D time-lapse movies

A total of 64 h of time-lapse video were analyzed. Movie files were modified (e.g. substacks made) to maximize manageability and facilitate manual annotation using Zen blue (Carl Zeiss, Oberkochen, Germany), Fiji (Schindelin et al., 2012), and/or Imaris (Bitplane, Zurich). Fiji and/or Imaris were used to assess three-dimensional morphology and track the locations of cells and clones over time, (e.g., ROI manager and MTrackJ in Fiji; Imaris Spots function). Cell division was categorized via classic morphological traits including rounding up of the cell soma at the apical surface, followed by cytokinesis and/or a corresponding increase in cell number within the clone. Cell cycle was calculated as the time that elapsed between two subsequent cell divisions of one progenitor cell. These times were averaged together for eight different clones followed in two fish. In order to clarify ambiguities related to cytokinesis, the frame of division was defined as the point at which two distinct spherical objects became clearly visible. In some cases, unambiguous mitotic figures

were not captured within the time interval; thus the subsequent frame was used as the time of division.

2.7. Quantifying clonal apoptosis

Apoptotic cells were characterized by a visible budding, blebbing, and "exploding" morphology accompanied by a corresponding decrease in cell number within the clone. For any observed apoptotic event, the time point and location of the cell were noted and any other clonal members were carefully tracked. In the event that only one cell in the clone underwent apoptosis during the period observed, the event was categorized as an "isolated apoptosis." If more than one, but not all, of the visible clonal members underwent apoptosis, each event was categorized as a "partial clonal apoptosis." If all members of the clone underwent apoptosis, each event was categorized as a "whole clonal apoptosis." For the apoptosis vs. time imaged graph (Fig. 4B), the number of observed cell deaths that occurred within an entire imaged hindbrain region was recorded at each hour interval (imaged at 30 min time points) in three different fish, then averaged together for each time point. Time of death was assigned to the time point in which the dying cell began to visibly bud and bleb. Monte Carlo simulation was done in R: A Language and Environment for Statistical Computing (Vienna, Austria; R Core team, 2017). We calculated the observed number of isolated cell deaths (only a single cell dying per clone) and clonal cell deaths (cells that died in a clone where at least one other cell also died) from three time-lapse imaging datasets. We then ran 10,000 simulations of populations of 346 clones, randomly sampling (with replacement) from the clone cell size distribution for a population of 346 clones. Each cell was assigned a fate (survive or die) using a binomial distribution with probability of death = 0.03, so that the probability of death was the same for every cell regardless of its clone identity. We then summed the number of total deaths in the simulated population, the number of clones experiencing the death of a single cell, and then number of clones experiencing the death of 2 or cells within the clone.

For apoptosis comparison to previous studies, the following logic was used for our *in vivo* data: Our current study identified 30 apoptotic events in 64 h of *in vivo* time-lapse, which is equivalent to 0.47 cells per hour; however, only ~5-10% of cells were labeled and thus visible in the tissue examined. Accounting for this, we estimate anywhere from (0.47)*10 or 4.7 to (0.47)*20 or 9.4 events occurring per hour. In van Ham et al. (2010), 40 apoptotic events were observed per hour in the entire brain. Assuming that the hindbrain makes up approximately 1/4 to 1/2 of total brain volume imaged in that study (estimated from images provided in Woo et al., 1995; van Ham et al., 2010), this can be adjusted to ~10–20 hindbrain cells per hour, which is slightly higher than our measurements. In Cole and Ross, 2001, four fixed time points were measured between 24-48 h. The authors reported that apoptotic cell clearance occurred in approximately 2 h. We used this information to estimate the rate of apoptosis at each of their time points, with each measurement representing approximately 2 h of time (see Table 1 below). The average of these rates was 5.584 cells per hour, which is slightly less than, but roughly similar to our measurements. For our fixed tissue caspase analysis, we calculated overall apoptosis levels by normalizing to volume and comparing to those values reported by Cole & Ross.

Table 1
Reported apoptosis values from Cole and Ross (2001), with estimated rate calculated.

Age	Number of apoptotic cells in hindbrain	Estimated rate of apoptosis
24 hpf	19.33 ± 10.07	19.33/2 h = ~9.665 cells/hour
30 hpf	2.67 +/2.08	2.67/2 h = ~1.335 cells/hour
36 hpf	15.00 ± 11.53	15.00/2 h = ~7.50 cells/hour
48 hpf	7.67 ± 8.96	7.67/2 h = ~3.835 cells/hour
	Average rate of apoptosis over 24 h period:	~5.584 cells/hour

2.8. Color analyses

Brainbow labeling density was calculated by co-staining with DAPI in fixed fish, counting the total number of cells in twelve different planes across three fish, and calculating the percent expressing Brainbow. Cell brightness for all color analyses was quantified using Fiji (Schindelin et al., 2012). For clonal color analysis, clusters in the hindbrain were selected by eye, using radial orientation and cell color as criteria, from both the full Z-stack and subset maximum intensity projections. Only cells captured entirely within the Z-stack that could be clearly distinguished from neighboring cells were included. For each cell of interest, the elliptical tool was used to select approximately the central 2/3 of the cell body in the central Z-plane of the cell; mean intensity measurements were taken for all three channels to give raw RGB values, using the same channel color coding used for on-screen display.

The RGB brightness for each cell was then converted to relative channel weight and displayed in ternary plots, as described in (Loulier et al., 2014). RGB cell brightness values were normalized by subtracting minimum background RGB intensity in the focal plane. Relative RGB channel weights were then calculated by dividing each channel's normalized cell brightness value by the total normalized brightness (sum of RGB values). Ternary plots displaying these relative channel weights as percentages were generated for each image analyzed using R: A Language and Environment for Statistical Computing and the Ternary package (Vienna, Austria; R Core team, 2017; Smith, 2017). For images in Fig. 1G only, three measurements of each cell's color were taken and the mean relative channel weights are displayed in Fig. 1H.

Color spread coefficient was defined as the normalized Euclidean distance between the color of two cells in three-dimensional (3D) RGB space. Normalization to values ranging from 0 to 1 for ease of comprehension was performed by dividing by $\sqrt{2}$, the maximal possible color distance:

$$distance = \sqrt{(R_1 - R_2)^2 + (G_1 - G_2)^2 + (B_1 - B_2)^2}$$

$$color\ spread\ coefficient = \frac{distance}{\sqrt{2}}$$

where R, G, and B are relative channels weights between 0 and 1.

For comparing the color spread between radial and non-radial cells, cell color data from the hindbrain of one fish was used (Fig. 1C_2 and E_2). Cells with ambiguous clonal/radial relationships were eliminated from the analysis; affecting roughly 20% of cells, typically in regions of overly dense labeling. Using R, the color spread coefficient was calculated for all pairwise combinations of cells and categorized as either "radially clustered cells" or "cells not radially clustered". The mean color spread coefficients for these groups were then compared via a Welch Two Sample *t*-test.

For FP brightness and apoptosis analysis (Fig. 4A), measures of fluorescence intensity were recorded from cells 60-65 min prior to apoptosis (depending on time-lapse interval). For each apoptotic cell measured within a time-lapse movie, paired control cells, from clones in which no cells were observed to undergo apoptosis, were selected and measured at the same time point as the corresponding apoptotic cell. All control cells with central planes within a range of five focal planes (3.4–4.5 μm) centered around the apoptotic cell that were visible by eye without brightness adjustments were sampled; depending upon Brainbow-labeling density, one to 14 control cells were selected per apoptotic cell. For each cell of interest, the elliptical tool was used to select as much area within the cell body as possible on the central plane of the cell; mean intensity measurements were taken for all three channels to give raw RGB values, using the same channel color coding used for on-screen display. All cell brightness measurements were normalized by subtracting mean background RGB values from the same time point and focal plane; background values were calculated by averaging RGB

measurements of five unlabeled hindbrain cells, selected via elliptical ROIs of 20-30 μm^2. Normalized RGB brightness values were converted to relative (or percent) RGB brightness values by dividing by the maximal intensity value of the image, allowing brightness comparisons between movies with varying bit depths. To give a total brightness value, relative RGB brightness values were summed for each cell.

2.9. Caspase analyses

To compare levels of apoptosis in the developing zebrafish hindbrain, images of both Brainbow-expressing and wild-type uninjected zebrafish hindbrains stained for activated caspase were analyzed in Fiji. The number of caspase-positive cells within the hindbrain was quantified by eye and normalized to volume to give a density of apoptotic events; volume imaged was calculated using the Measure Stack plug-in (Opti-Nav). Overall hindbrain volume was measured using Imaris from transmitted light images. Two-way ANOVA in R was used to test for significant effects of age, construct, and their interaction on levels of apoptosis in the zebrafish hindbrain. Tukey's HSD test was then performed in R to make pairwise comparisons between conditions.

3. Results

3.1. Brainbow distinguishes dividing clones over time in vivo

To begin to investigate clonal dynamics in the developing zebrafish brain, we stochastically expressed Brainbow (Hsp:Zebrabow; Fig. 1A) in zebrafish embryos by DNA injection at the one-cell stage, and performed *in vivo* time-lapse confocal microscopy at 1-3 days post fertilization (dpf; Fig. 1B-C). We focused our analysis on the developing hindbrain (Moens and Prince, 2002), which is readily visible in the living larval zebrafish (Fig. 1B_1), and where overall rates of cell division and apoptosis have been characterized (Trevarrow et al., 1990; Cole and Ross, 2001; Lyons et al., 2003; van Ham et al., 2010). We used transient DNA injections and 24 hpf heat shock activation (Fig. 1B_2) to titrate the density and color diversity of Brainbow labeling. Our labeling density ranged from approximately 4-15% of cells within the hindbrain (e.g., Fig. 1C–D), a fraction that was ideal for visualizing a large number of individual cells. The labeled cell population expressed an array of colors that ranged throughout the visible spectrum (Fig. 1E), thus it was relatively straightforward to distinguish neighboring cells from one another. When multiple cells were clustered along a given radial fiber, however, they typically expressed the same color, suggesting that radial clones of dividing cells were sharing a similar hue that could identify them as being clonally related, e.g., derived from the same mother cell, similar to previous studies in zebrafish, mouse, and chick (Pan et al., 2013; Loulier et al., 2014). The color-coding, coupled with the relatively sparse labeling density, allowed for unambiguous distinction of neighboring cell clusters.

To test whether color could be used to distinguish radial clusters of cells from one another, we quantified red, green, and blue (RGB) intensity values in individual cells and plotted this in three-dimensional (3D) color space (Fig. 1F; Loulier et al., 2014). Difference in color was measured as a coefficient value that represented the distance between cells in 3D RGB space (difference in red, difference in green, and difference in blue). The color expressed within radial clusters of cells was similar enough to unambiguously separate them from neighboring clusters, with the mean color spread coefficient within radial clusters being 0.027 ± 0.023 (out of 1), while non-radially oriented cells had a significantly larger mean color spread coefficient of 0.240 ± 0.142 (Fig. 1F; Welch Two Sample *t*-test, $t(648.66)=170.59$, $p < 2.2 \times 10^{-16}$). Color-coded clusters at 30 hpf consisted of 2 to 5 cells typically oriented along a radial fiber, consistent with being clones derived from radial glial progenitor cells (Noctor et al., 2001; Lyons et al., 2003). To confirm that these color-coded clusters of cells were clonally related to one another, we followed individual cell divisions over time and quantified the color expressed within mother and daughter cells (Pan et al., 2013; Loulier et al., 2014). Daughter cells expressed the same color as their mother (progenitor) cell (Fig. 1G-H). In the example shown, the daughter cells differed by a color spread coefficient of 0.012; each differed from its mother cell by 0.017 and 0.024, demonstrating that color remained relatively constant during cell division within a clone. Each radially oriented, color-coded cluster of cells was thus considered a group of clonally related cells that had derived from a common mother cell. These data show that Brainbow effectively color-codes clones of dividing cells in the living zebrafish brain, and that multicolor expression can be used for a "multi-clonal analysis" – the tracking of numerous individual neighboring clones of dividing cells simultaneously.

To test whether color-coded clones could be followed over periods of time *in vivo*, we imaged living fish and quantified color expression in clones at 2 dpf and then again at 3 dpf (Fig. 2A). Overall color expression throughout the hindbrain was similar from one day to the next (Fig. 2B). The color expressed within individual clonal members, which again clustered in three-dimensional RGB space, was distinct from neighboring clones, and remained relatively constant from 2 to 3 days *in vivo*. These data demonstrate that multiple distinct clones of dividing cells can be followed over time *in vivo*.

We next followed clonal dynamics over time by performing *in vivo* imaging sessions with shorter time intervals in Brainbow-expressing zebrafish from 24 to 48 hpf. Due to the many colors expressed throughout the brain, multiple dividing clones could be followed simultaneously within a given field, and quantified across the region imaged (Fig. 2C–F). As expected, cells underwent interkinetic nuclear migration based on directional movements (Sauer, 1935; Norden et al., 2009; Meyer et al., 2011), typically entering mitosis and dividing at the apical (ventricular) surface (Fig. 2D, F). We were able to quantify cell division dynamics in multiple different clones simultaneously; of the 104 clones followed (each for approximately 11 h), 63 underwent at least one apical cell division, and some underwent two divisions, allowing us to measure cell cycle times. Since our time-lapse interval was 30 min, we did not always capture mitotic figures, thus the assigned time of division contains a potential error of up to 30 min. Further, some clones appeared to contain two progenitor cells (Fig. 2F). By following individual progenitors over time we calculated an average cell cycle of 8.4 ($\pm$1.5) hours, which is in line with previous zebrafish reports (Lyons et al., 2003; Baye and Link, 2007; Leung et al., 2012).

3.2. Dividing clones undergo coordinated cell death

Using our Brainbow labeling and imaging strategy we were also able to detect individual cells undergoing the stereotypical morphological changes associated with apoptosis (Fig. 3A-B), including membrane blebbing and cell fragmentation (Kerr et al., 1972). Simultaneous image acquisition in the transmitted light channel confirmed that individual cells were dying while neighboring cells (both labeled and unlabeled with Brainbow) appeared morphologically normal. In ~64 h of time-lapse video analyzed from four different fish (29–48 hpf), we detected 30 cells undergoing apoptosis. This frequency is within the range that would be expected based on previous quantifications of apoptosis in zebrafish hindbrain (Cole and Ross, 2001; Lyons et al., 2003; van Ham et al., 2010), which is known to peak from 22 to 36 hpf (Cole and Ross, 2001); see Table 1 and Discussion).

Since Brainbow expression color coded clones of dividing cells and allowed for a multi-clonal analysis, we next used our long-term time-lapse imaging experiments to quantify apoptosis patterns among and within clones over time. Interestingly, apoptosis did not occur in a random manner. On the contrary, members of an individual clone sometimes underwent apoptosis in a coordinated pattern, with one cell dying, then subsequent members of the same clone dying in a progressive fashion (Fig. 3C-D). We termed this behavior "clonal apoptosis". The stereotyped sequence always began with one lone cell undergoing

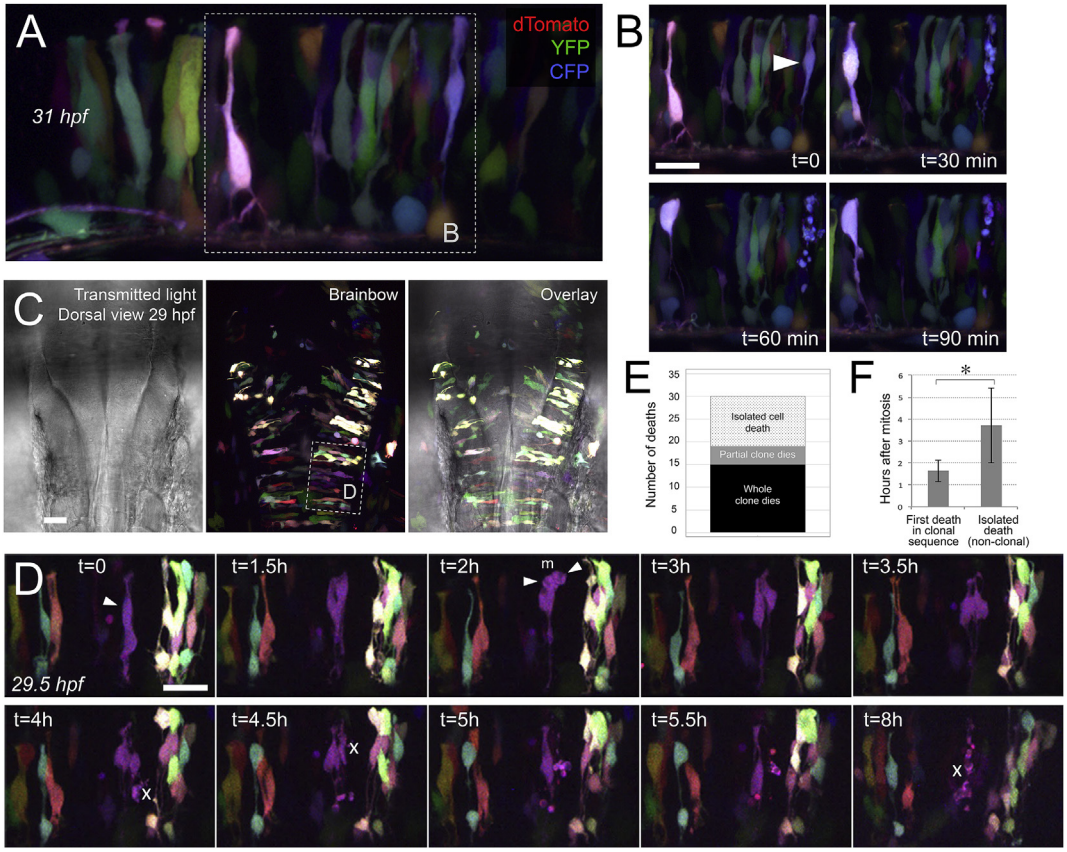

Fig. 3. Cells within dividing clones in the ventricular zone undergo coordinated death *in vivo*.
A) Zebrafish hindbrain at 31 hpf labeled with Brainbow (maximum intensity projection representing 36μm). White dashed box indicates inset shown in the first time point in B. B) Series of time points showing hindbrain in A at 30-min intervals. White arrowhead in first panel shows lavender cell that will undergo apoptosis in subsequent panels, indicated by cell fragmentation followed by gradual clearance of apoptotic bodies. Neighboring labeled cells appeared healthy throughout. Dorsal is up and rostral is to the left. C) Dorsal view of 29 hpf zebrafish hindbrain labeled with Brainbow; transmitted light channel shows the morphology of hindbrain and ventricle, overlaid with maximum intensity projection of Brainbow-labeled clones representing 165μm. Rostral is up. White dashed box indicates region shown zoomed and rotated in D. D) Series of time points of hindbrain from C taken at 30 min intervals (maximum intensity projections of 30μm). Over a period of 8h, the purple clone can be observed first undergoing mitosis (indicated by white arrowheads), before undergoing progressive whole-clone apoptosis (apoptotic events indicated by white "X"). Throughout this stepwise apoptotic process, nearby labeled cells appear healthy. Rostral is to the right. Scale bar represents 20μm in B, 30μm in C and 20μm in D. E) Number of cell deaths from *in vivo* time-lapse movies, categorized as isolated cell death, partial-clone apoptosis, or whole-clone apoptosis (n=30 deaths). The majority of deaths observed (19/30) are clonal. F) Mean time elapsed between mitosis and apoptosis, for isolated cell deaths (n=6 cells from 3 fish) and the first death in clonal apoptosis sequence (n=4 cells from 3 fish); error bars represent standard deviation; $p < 0.05$. In all Brainbow images, dTomato is coded as red, YFP is coded as green, and CFP is coded as blue.

apoptosis. Often this occurred in a daughter cell within 1-3 h following mitosis at the ventricular surface (Fig. 3D and see below). The first death was followed within 1-3 h by the loss of a second cell from the same clone (mean 1.7 ± 1.1 h), and then more rapid loss of the remaining clone members (usually within 30 min). Most of the apoptosis we tracked *in vivo* followed this stereotyped clonal pattern (Fig. 3E): of the 30 apoptosis events observed in 64 h of time-lapse, 19 were clonal, occurring within clones such that multiple clonal members were lost. In 15 of these clonal deaths, we detected the loss of all clone members (termed "whole-clone apoptosis"). In the remaining 4 clonal events, multiple members of a clone underwent apoptosis, but we did not capture the loss of all remaining clone members ("partial-clone apoptosis"). Only eleven of the 30 deaths we tracked overall occurred in a seemingly random way, affecting single dispersed cells dying at unrelated time points. A Monte-Carlo simulation showed that it was unlikely that 19 out of 30 apoptosis events occurring within clones was due to chance (Supplemental Fig. 1). Some isolated deaths classified as non-clonal occurred in the first or last few hours of image collection; thus we cannot rule out the possibility that these isolated events were in fact part of a longer clonal event. Because of this, we may have underestimated the proportion of clonal events. Importantly, apoptosis events occurred within the same field as other clones that appeared normal and continued to divide during the same time period.

We next asked which cells initiated the clonal apoptotic events, and whether apoptosis was correlated with a particular point in the cell cycle. Since dividing cells in the ventricular epithelium undergo interkinetic nuclear migration, cell cycle phase is directly related to somatic position within the ventricular zone, whereby cells in the basal region undergo S-phase while cells enter mitosis at the apical ventricular surface (Sauer, 1935; Norden et al., 2009). Furthermore, previous studies have shown that the daughter cell that is positioned more apically following asymmetric division begins to express early neural differentiation markers, suggesting that it is the neuronal daughter cell (Alexandre et al., 2010). In our measurements of clonal apoptosis, there was not a consistent apical or basal location of the first cell to die; it could be located either apically, basally, or level with other cells in the clone. Thus it is not clear from our data if the death sequence is initiated by a daughter cell or a cycling progenitor. Although we did not always capture mitosis before a clonal event, when mitosis was observed, the first death occurred within several hours after mitosis (Fig. 3F; mean 1.6 ± 0.5 h for deaths that

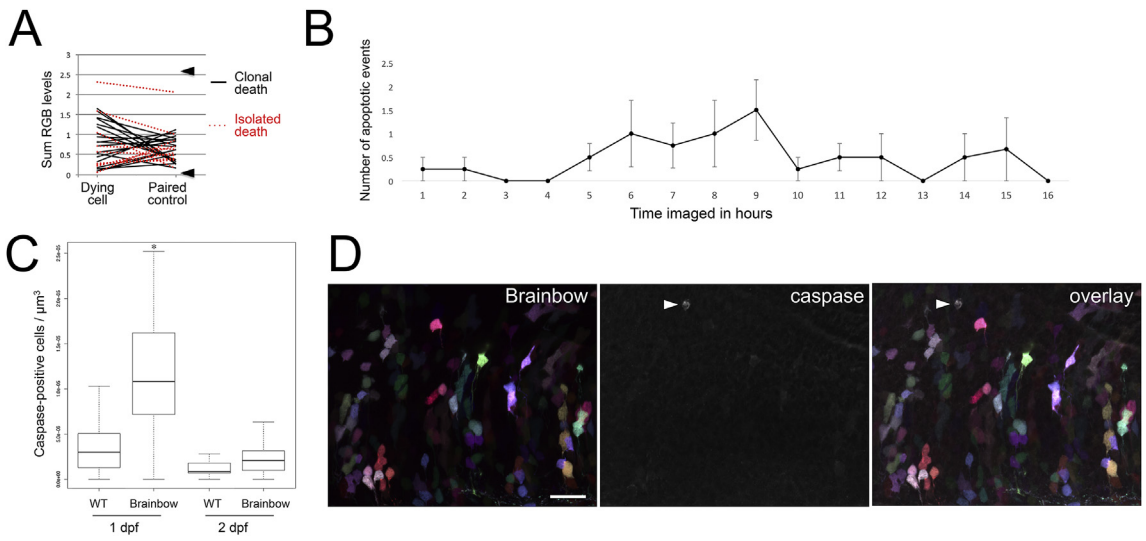

Fig. 4. Brainbow expression does not cause clonal apoptosis.
A) The brightness of cells that undergo apoptosis paired with the brightest neighboring control cell; brightness is quantified by summed relative RGB value (range of 0 to 3; n=30 cells/condition from 4 fish). Solid black lines represent brightness differences when the dying cell is part of a clonal apoptosis event and dashed red lines represent cases in which the dying cell is an isolated death. Arrowheads show the overall range of healthy control cells in the same tissue. B) Mean number of apoptotic events observed in hindbrain over time imaged; error bars represent standard error of the mean; n=4 fish. C) Quantified activated caspase-positive cells in fish expressing Brainbow following injection and heat shock, and in uninjected, wild-type fish at both 1 dpf (Brainbow: n=23 fish, WT: n=16 fish) and 2 dpf (Brainbow: n=29 fish, WT: n=40 fish). Whiskers represent extremes of data. D) 48 hpf zebrafish hindbrain expressing Brainbow (maximum intensity projection of 29µm); caspase staining is coded as white for display. Dorsal is up and rostral is to the left; scale bar represents 20µm. In D, dTomato is coded as red, YFP is coded as green, and CFP is coded as blue.

initiated clonal apoptosis versus 3.7 ± 1.7 h for isolated, non-clonal deaths that followed mitosis; $p < 0.05$). Depending upon whether the identity of this first dying clone member was neuronal or a progenitor cell continuing to cycle, it may be in G1, entering S, or entering G0 at this time point (Leung et al., 2012). We never observed mitosis in a clone following the death of one of its members.

3.3. Clonal apoptosis is not caused by brainbow expression

Under some circumstances fluorescent proteins can cause cellular toxicity (Ansari et al., 2016; but see Taghizadeh and Sherley, 2008, who suggest that CFP and YFP may be less toxic than GFP). Therefore, we next tested whether the clonal apoptosis events we identified were caused by Brainbow expression within a given clone. To test for potential fluorescent protein toxicity, we used a battery of analyses measuring fluorescence intensity, behavior under imaging conditions, and activated caspase expression.

We first reasoned that if Brainbow expression influences clonal apoptosis, we would expect cell death to occur more often in brighter clones (exhibiting higher fluorescent protein levels). Qualitatively, however, this did not appear to be the case, since clonal apoptosis could occur in dimly expressing clones (e.g. Fig. 3D). To test this quantitatively, we measured the RGB fluorescence intensity in healthy clones versus clones undergoing clonal apoptosis, quantifying the intensity of each channel individually. Since brightness varies across fish, we compared each cell to a paired group of neighboring cells sampled across the hindbrain within a depth of 3.4–4.5 µm around the apoptotic cell. Dying cells were equally likely to be dimmer than their brightest neighboring cells (15/30 cells) as they were to be brighter (15/30; Fig. 4A). Even the brightest cells that died were well within the range of brightness levels measured in healthy cells across the hindbrain (~0.05–2.62 AU; arrowheads show approximate range of healthy controls in Fig. 4A). Cells undergoing apoptosis thus expressed Brainbow at levels similar to healthy control cells sampled within the same region. This suggests that clonal apoptosis is not triggered by increased levels of Brainbow expression.

We next tested whether time-lapse imaging itself had an effect on cell survival. We reasoned that if our imaging conditions were inducing phototoxicity and/or triggering apoptotic events, the frequency of deaths should increase with the length of the imaging session. This was not the case, however. Average frequency measurements over time (Fig. 4B) showed that clonal apoptosis was as likely to occur in the first frame of a time-lapse imaging session as in the final (sixteenth) hour of imaging.

Finally, we tested whether Brainbow expression was influencing apoptosis by measuring activated caspase activity within the hindbrain of injected and wild-type uninjected fish. We used immunohistochemistry against activated caspase to quantify apoptosis and found there were lower caspase levels at 1 dpf in uninjected wild-type fish versus those that were injected with Brainbow DNA then heat shocked to activate transcription (Fig. 4C; 1.15×10^{-5} +/- 0.67×10^{-5} cells/µm^3 versus 3.55×10^{-6} +/- 2.92×10^{-6} cells/µm^3 in wild-type; $F_{1,104}=23.24$, $p < 1.0 \times 10^{-5}$; Tukey HSD $p < 1.0 \times 10^{-4}$). At 2 dpf, however, caspase levels were similar in wild-type fish versus those injected with Brainbow and heat-shocked (2.38×10^{-6} +/- 1.84×10^{-6} cells/µm^3 versus 1.31×10^{-6} +/- 1.45×10^{-6} cells/µm^3 in wild-type; Tukey HSD $p > 0.5$). We normalized these counts to overall hindbrain volume, and found that our quantification of caspase levels in 1 dpf wild-type fish and at 2 dpf for both wild-type and Brainbow expressing fish is roughly similar to previous reports in wild-type hindbrain (Cole and Ross, 2001; Lyons et al., 2003; van Ham et al., 2010). This suggests that DNA injection, heat-shock, and Brainbow expression do not affect apoptosis at 2 dpf, but may increase apoptosis at 1 dpf. When caspase levels were analyzed within Brainbow-expressing hindbrain at both ages, the majority of caspase-positive cells (71.6%) were not expressing Brainbow (e.g., Fig. 4D). While exogenous Brainbow expression and heat shock activation may increase overall apoptosis levels in 1 dpf embryos, it is thus unlikely that the stereotyped clonal apoptosis sequence that we observe in Brainbow-labeled clones over hours *in vivo* are caused by fluorescent protein toxicity or by time-lapse imaging conditions. We cannot rule out the possibility that some of the observed isolated deaths were due to these conditions, but taken together

our results suggest that clonal apoptosis is likely a natural part of zebrafish neural development.

4. Discussion

Here we use a multicolor *in vivo* approach to demonstrate for the first time a coordinated pattern of apoptosis in the developing hindbrain, whereby multiple cells within a given clone die in succession. Within several hours following mitosis, a cell within the dividing clone undergoes the classical signs of apoptosis and disappears; the other cells in its clone, including its own mother cell, can also undergo apoptosis in successive order over the next several hours. Clonal apoptosis is not caused by *in vivo* time-lapse imaging conditions, and is not correlated with Brainbow expression levels *in vivo*. Further, apoptosis frequency measured *in vivo* is consistent with previous findings in the zebrafish hindbrain at this stage of development. Our results suggest that coordinated apoptosis within clones is a feature of normal brain development.

4.1. Why hasn't clonal apoptosis been detected previously in the vertebrate brain?

Clonal apoptosis in the vertebrate brain has not been reported previously, despite numerous elegant studies that have used a clonal analysis approach (Luskin et al., 1988; Price and Thurlow, 1988; Walsh and Cepko, 1992, 1993; Cai et al., 1997; Reznikov et al., 1997; Qian et al., 1998; McCarthy et al., 2001; Noctor et al., 2001; Yu et al., 2009). The unique combination of Brainbow clonal labeling and *in vivo* time-lapse imaging in zebrafish may be critical to observe this phenomenon. Important studies that have labeled individual radial glial cells and their progeny using low titers of retrovirus expressing a single fluorescent protein have tracked the behavior of single clones, but have not been able to identify multiple clones simultaneously and/or study coordinated mechanisms *among* clones. The likelihood of labeling a clone that is undergoing clonal apoptosis using single or dual clone labeling techniques is very low (we observed on average two dying clones per hindbrain per 11 h), and would require time-lapse imaging of brain regions over many hours. Mammalian brain slices, however, allow for visualization of only a small portion of the brain. Furthermore, even if observed, such apoptosis may be attributed to unfavorable slice culture conditions and ignored. We have optimized Brainbow in zebrafish, an important model for vertebrate development (Ingham, 1997; Wullimann and Mueller, 2004; Howe et al., 2013), to obtain distinct labeling of many individual hindbrain clones and follow them *in vivo* during normal embryonic development (1–3 dpf). The translucency of zebrafish at these ages provides a window into early neural development that is more difficult to obtain in mammals (Fetcho and Liu, 1998; Lyons et al., 2003; Hocking et al., 2013; Yanakieva et al., 2018).

One might expect that clonal apoptosis could have been identified in fixed tissue analysis, which has been used to study apoptosis in development (e.g. Cole and Ross, 2001). Our time-lapse recordings show, however, that the sequence of cell deaths in a clone typically occurs over multiple hours; each dying cell may be cleared away by the time subsequent cells in the clone begin to apoptose (estimated 2 h for clearance; Cole and Ross, 2001). Given this timing, it would be difficult to capture simultaneous caspase expression or TUNEL staining in multiple clonal members at one fixed time point. In at least one study in the hindbrain, however, small clusters of TUNEL-positive cells were visible (Cole and Ross, 2001), although the methods in that study did not allow for identification of clones.

The observed frequency of apoptosis in our *in vivo* time-lapse movies is consistent with previous studies that have measured this frequency in the zebrafish hindbrain (Cole and Ross, 2001; Lyons et al., 2003; van Ham et al., 2010; see Table 1 and Methods). Thus the levels of apoptosis we have observed *in vivo* are within the range of normal, healthy development. The levels of apoptosis that we measured via fixed tissue analysis showed that caspase levels were increased compared to control in 1 dpf fish that were expressing Brainbow following a heat shock step. The heat shock step needed for Brainbow transcription occurs just before the 1 dpf time point, thus fish at 1 dpf are likely more sensitive to and potentially still recovering from heat shock when they were fixed. This might be expected to increase generalized, random cell death – but not the patterned, step-wise events that we have observed in clones. Furthermore, most caspase-positive cells were Brainbow-negative, indicating that Brainbow expression itself did not cause these events. Moreover, we observed a large population of healthy, dividing clones labeled with Brainbow. A small fraction of those clones died – mostly in a clonal pattern (19 out of 30), from 30 to 46 hpf. It is unlikely that the patterned clonal events were the result of a generalized toxicity to the tissue.

4.2. Why are clonally related cells dying?

Clones of cells have been shown to undergo coordinated apoptosis in the *Drosophila* wing imaginal disc (Morata and Ripoll, 1975; Simpson, 1979; Simpson and Morata, 1981). A series of elegant studies has established that this coordination can be caused by competition of clones of cells with varying fitness levels (reviewed in Merino et al., 2016). The more fit clones survive and "win", while less fit clones "lose", dying by apoptosis. Cell competition has also been shown to occur in multiple vertebrate systems during development, such as the early mouse embryo (Clavería et al., 2013; Sancho et al., 2013), heart (Villa del Campo et al., 2014), skin (Walderich et al., 2016), blood (Micklem et al., 1972), germ line cells and others (Stoner et al., 2002; Weissman, 2015). Cellular fitness can be conferred by a number of identified factors such as access to the extracellular factor decapentaplegic factor (DPP) in flies or bone morphogenetic protein (BMP) in mammals (Moreno et al., 2002; Sancho et al., 2013), or intrinsic factors such as Myc (De La Cova et al., 2004; Moreno and Basler, 2004; Clavería et al., 2013; Villa del Campo et al., 2014), both of which are present in the nervous system. In fish, clonal dominance has been seen in the heart (Gupta and Poss, 2012) and skeletal muscle (Nguyen et al., 2017). We also observed large clones of neurons in the juvenile zebrafish tectum (Pan et al., 2013), which could be a result of clonal competition.

A pattern of clonal competition has not been detected previously in the brain, although developing neurons rely upon extracellular factors for survival (Jessell and Sanes, 2000) and it has long been hypothesized that they compete for such factors, originally proposed in the neurotrophic hypothesis (Levi-Montalcini, 1987). Competition among neurons has been well established as a critical mechanism for refining innervation of postsynaptic targets (Purves and Lichtman, 1980; Katz and Shatz, 1996; Zhang et al., 1998; Sanes and Lichtman, 1999; Hashimoto et al., 2009; Feldheim and O'Leary, 2010). Our findings suggest that cells may compete in the developing brain not only at the level of the individual cell but at the level of whole clones. This raises an interesting set of questions about what molecular factors may determine clone fitness, and what specific resources clones may be competing for. Borrowing from work done in flies, intriguing candidates to test would be bone morphogenetic protein as well as Myc.

It is not clear what, if anything, is potentially different between two neighboring, competing clones in the proliferative ventricular zone of an individual brain. In the *Drosophila* work on clonal cell competition, winners and losers are dictated by clear genetic differences between dividing clones of cells (e.g. Morata and Ripoll, 1975). In zebrafish hindbrain, the underlying genome is theoretically identical among neighboring neuronal progenitors. *De novo* mutations resulting from replication errors during S-phase, however, may arise during radial glial cell proliferation and be propagated to a mother cell's clone. Furthermore, epigenetic modifications that occur in proliferating radial glia have been shown to be critical for proper development, influencing the expression of genes involved in neurogenesis and the migration of newly differentiating neuronal progeny (Baizabal et al., 2018). Indeed, chromatin remodeling is critical in some developmental disorders

(Mastrototaro et al., 2017). Epigenetic differences or genetic differences due to clone-specific mutations could thus result in divergence between neighboring clones of cells, and ultimately improved fitness in one of them, perhaps through increased or decreased access to extracellular growth factors (Raff, 1992; Yeo and Gautier, 2004).

4.3. How do cells in a clone communicate the 'death signal'?

Because up to four cells within the same clone can undergo apoptosis in a coordinated manner, we hypothesize that there must be a "death signal" of some sort shared among these cells. A unitary signal received by all cells at once seems unlikely, because the clonal members die one by one in a successive manner over several hours, not simultaneously. This sequence is instead suggestive of a signal that passes from one cell to the next, perhaps released as a dying cell begins the cascade of apoptotic factor activation. Indeed, cell-cell contact is known to be critical for competition among clones (Merino et al., 2016), and directional intercellular signaling has been observed between clonally related cells (Dong et al., 2012). Since radial glial cells are gap-junction-coupled in the ventricular zone (Lo Turco and Kriegstein, 1991; Bittman et al., 1997); one possible mechanism of communication may be via gap junction channels. Another possibility is the release of a signaling factor via connexin hemichannels (Bennett et al., 2003), which are known to also be functional in the ventricular zone and important for calcium signaling among radial glial cells (Weissman et al., 2004).

One clue may be that the origin of the signal appears to come during or following mitosis at the ventricular surface. We find that in most cases, the first death occurs within several hours following a mitotic cell division, potentially implicating the G1 checkpoint. Cell cycle mutants may show varying degrees of clonal apoptosis and could be used to test this possibility. The use of a nuclear marker (Alexander et al, 2010), a shorter time-lapse interval, and potential co-expression of a neuron- or progenitor-specific signal will aid in unambiguous identification of which cell may be initiating the cascade of apoptosis within a clone – cycling progenitor and/or daughter cell.

4.4. Model of brain development

Here we show that clonally related cells in the developing hindbrain undergo coordinated cell death, while neighboring clones continue to divide and populate the growing tissue. Clonal apoptosis could represent a conserved, basic mechanism that helps to regulate the number of neural progenitor cells available for neuronal production in the vertebrate nervous system. If regulated by extracellular resources, the number of surviving clones would naturally match the resources available for growth in that particular brain region, providing a parsimonious mechanism for size regulation. Clones of dividing cells may thus compete with one another for survival: less fit clones lose and undergo coordinated clonal apoptosis. There are intriguing next steps to test in this system, for example, manipulating expression of specific gene candidates to test whether relative fitness of individual clones can influence their likelihood to survive.

Acknowledgements

We thank Jean Livet for sharing tools for generating ternary plots and for helpful discussions; Alia Newman-Boulle and Talia Lichtenberg for technical assistance; and Kara Cerveny for sharing embryos and for helpful discussions. This work was supported by the National Science Foundation (Award 1553764), the M.J. Murdock Charitable Trust, and the John S. Rogers Research Program at Lewis & Clark College.

Appendix A. Supplementary data

Supplementary data to this article can be found online at https://doi.org/10.1016/j.ydbio.2019.05.006.

References

Alexandre, P., Reugels, A.M., Barker, D., Blanc, E., Clarke, J.D.W., 2010. Neurons derive from the more apical daughter in asymmetric divisions in the zebrafish neural tube. Nat. Neurosci. 13, 673–679.
Ansari, A.M., Ahmed, A.K., Matsangos, A.E., Lay, F., Born, L.J., Marti, G., Harmon, J.W., Sun, Z., 2016. Cellular GFP toxicity and immunogenicity: potential confounders in in vivo cell tracking experiments. Stem Cell Rev Reports 12, 553–559.
Baizabal, J.M., Mistry, M., García, M.T., Gómez, N., Olukoya, O., Tran, D., Johnson, M.B., Walsh, C.A., Harwell, C.C., 2018. The epigenetic state of PRDM16-regulated enhancers in radial glia controls cortical neuron position. Neuron 98, 945–962 e8.
Baye, L.M., Link, B.A., 2007. Interkinetic nuclear migration and the selection of neurogenic cell divisions during vertebrate retinogenesis. J. Neurosci. 27, 10143–10152.
Bennett, M.V.L., Contreras, J.E., Bukauskas, F.F., Sáez, J.C., 2003. New roles for astrocytes: gap junction hemichannels have something to communicate. Trends Neurosci. 26 (11), 610–617.
Bittman, K., Owens, D.F., Kriegstein, A.R., LoTurco, J.J., 1997. Cell coupling and uncoupling in the ventricular zone of developing neocortex. J. Neurosci. 17 (18), 7037–7044.
Bolz, J., Novak, N., Götz, M., Bonhoeffer, T., 1990. Formation of target-specific neuronal projections in organotypic slice cultures from rat visual cortex. Nature 346, 359–362.
Cai, L., Hayes, N.L., Nowakowski, R.S., 1997. Synchrony of clonal cell proliferation and contiguity of clonally related cells: production of mosaicism in the ventricular zone of developing mouse neocortex. J. Neurosci. 17, 2088–2100.
Caviness, V.S., Takahashi, T., Nowakowski, R.S., 1995. Numbers, time and neocortical neuronogenesis: a general developmental and evolutionary model. Trends Neurosci. 18, 379–383.
Chenn, A., McConnell, S.K., 1995. Cleavage orientation and the asymmetric inheritance of notchl immunoreactivity in mammalian neurogenesis. Cell 82 (4), 631–641.
Clavería, C., Giovinazzo, G., Sierra, R., Torres, M., 2013. Myc-driven endogenous cell competition in the early mammalian embryo. Nature 500, 39–44.
Cole, L.K., Ross, L.S., 2001. Apoptosis in the developing zebrafish embryo. Dev. Biol. 240 (1), 123–142.
Conlon, I., Raff, M., 1999. Size control in animal development. Cell 96, 235–244.
Cook, Z.T., Brockway, N.L., Tobias, Z.J.C., Pajarla, J., Boardman, I.S., Ippolito, H., Nkombo Nkoula, S., Weissman, T.A., 2018. Combining near-infrared fluorescence with Brainbow to visualize expression of specific genes within a multicolor context. Mol Biol Cell:mbc. E18–06, 0340.
Corbin, J.G., Gaiano, N., Juliano, S.L., Poluch, S., Stancik, E., Haydar, T.F., 2008. Regulation of neural progenitor cell development in the nervous system. J. Neurochem. 106, 2272–2287.
Dammerman, R.S., Noctor, S.C., Kriegstein, A.R., 2000. Extrinsic GABAergic innervation of developing neocortical layer 1 in organotypic slice co-cultures. J. Comp. Neurol. 423 (1), 112–120.
De La Cova, C., Abril, M., Bellosta, P., Gallant, P., Johnston, L.A., 2004. Drosophila myc regulates organ size by inducing cell competition. Cell 117, 107–116.
Dong, Z., Yang, N., Yeo, S.Y., Chitnis, A., Guo, S., 2012. Intralineage directional notch signaling regulates self-renewal and differentiation of asymmetrically dividing radial glia. Neuron 74, 65–78.
Dzafic, E., Strzyz, P.J., Wilsch-Bräuninger, M., Norden, C., 2015. Centriole amplification in zebrafish affects proliferation and survival but not differentiation of neural progenitor cells. Cell Rep. 13, 168–182.
Feldheim, D.A., O'Leary, D.D.M., 2010. Visual map development: bidirectional signaling, bifunctional guidance molecules, and competition. Cold Spring Harb Perspect Biol 2 (11), a001768.
Fetcho, J.R., Liu, K.S., 1998. Zebrafish as a model system for studying neuronal circuits and behavior. In: Annals of the New York Academy of Sciences, pp. 333–345.
Florio, M., Huttner, W.B., 2014. Neural progenitors, neurogenesis and the evolution of the neocortex. Development 141, 2182–2194.
Gupta, V., Poss, K.D., 2012. Clonally dominant cardiomyocytes direct heart morphogenesis. Nature 484, 479–484.
Hansen, D.V., Lui, J.H., Parker, P.R.L., Kriegstein, A.R., 2010. Neurogenic radial glia in the outer subventricular zone of human neocortex. Nature 464 (7288), 554–561.
Hashimoto, K., Ichikawa, R., Kitamura, K., Watanabe, M., Kano, M., I., 2009. Translocation of a "winner" climbing fiber to the purkinje cell dendrite and subsequent elimination of "losers" from the soma in developing cerebellum. Neuron.
Haydar, T.F., Bambrick, L.L., Krueger, B.K., Rakic, P., 1999. Organotypic slice cultures for analysis of proliferation, cell death, and migration in the embryonic neocortex. Brain Res. Protoc. 4 (3), 425–437.
Hocking, J.C., Distel, M., Köster, R.W., 2013. Studying cellular and subcellular dynamics in the developing zebrafish nervous system. Exp. Neurol. 242, 1–10.
Homem, C.C.F., Repic, M., Knoblich, J.A., 2015. Proliferation control in neural stem and progenitor cells. Nat. Rev. Neurosci. 16.
Howe, K., et al., 2013. The zebrafish reference genome sequence and its relationship to the human genome. Nature 496, 498–503.
Ingham, P.W., 1997. Zebrafish genetics and its implications for understanding vertebrate development. Hum. Mol. Genet. 6, 1755–1760.
Jessell, T.M., Sanes, J.R., 2000. Development: the decade of the developing brain. Curr. Opin. Neurobiol. 10, 599–611.
Katz, L.C., Shatz, C.J., 1996. Synaptic activity and the construction of cortical circuits. Science 80.
Kerr, J.F.R., Wyllie, A.H., Currie, A.R., 1972. Apoptosis: a basic biological phenomenon with wide-ranging implications in tissue kinetics. Br. J. Canc. 26 (4), 239–257.
Kriegstein, A., Alvarez-Buylla, A., 2009. The glial nature of embryonic and adult neural stem cells. Annu. Rev. Neurosci. 32, 149–184.

Kuan, C.Y., Roth, K.A., Flavell, R.A., Rakic, P., 2000. Mechanisms of programmed cell death in the developing brain. Trends Neurosci. 23 (7), 291–297.
Letinic, K., Rakic, P., 2001. Telencephalic origin of human thalamic GABAergic neurons. Nat. Neurosci. 4 (9), 931–936.
Leung, L., Klopper, A.V., Grill, S.W., Harris, W.A., Norden, C., 2012. Apical Migration of Nuclei during G2 Is a Prerequisite for All Nuclear Motion in Zebrafish Neuroepithelia. Development.
Levayer, R., Moreno, E., 2013. Mechanisms of cell competition: themes and variations. J. Cell Biol. 200, 689–698.
Levi-Montalcini, R., 1987. The nerve growth factor 35 years later. Science 80.
Livet, J., Weissman, T a, Kang, H., Draft, R.W., Lu, J., Bennis, R a, Sanes, J.R., Lichtman, J.W., 2007. Transgenic strategies for combinatorial expression of fluorescent proteins in the nervous system. Nature 450, 56–62.
Lo Turco, J.J., Kriegstein, A.R., 1991. Clusters of coupled neuroblasts in embryonic neocortex. Science (80–) 252 (5005), 563–566.
LoTurco, J.J., Sarkisian, M.R., Cosker, L., Bai, J., 2003. Citron kinase is a regulator of mitosis and neurogenic cytokinesis in the neocortical ventricular zone. Cerebr. Cortex 13 (6), 588–591.
Loulier, K., Barry, R., Mahou, P., Franc, Y Le, Supatto, W., Matho, K.S., Ieng, S., Fouquet, S., Dupin, E., Benosman, R., Chédotal, A., Beaurepaire, E., Morin, X., Livet, J., 2014. Multiplex cell and lineage tracking with combinatorial labels. Neuron 81, 505–520.
Lui, J.H., Hansen, D.V., Kriegstein, A.R., 2011. Development and evolution of the human neocortex. Cell 146, 18–36.
Luskin, M.B., Pearlman, A.L., Sanes, J.R., 1988. Cell lineage in the cerebral cortex of the mouse studied in vivo and in vitro with a Recombinant Retrovirus. Neuron 1, 635–647.
Lyons, D.A., Guy, A.T., Clarke, J.D.W., 2003. Monitoring neural progenitor fate through multiple rounds of division in an intact vertebrate brain. Development 130, 3427–3436.
Malatesta, P., Hartfuss, E., Götz, M., 2000. Isolation of radial glial cells by fluorescent-activated cell sorting reveals a neuronal lineage. Development 127 127, 5253–5263.
Mastrototaro, G., Zaghi, M., Sessa, A., 2017. Epigenetic mistakes in neurodevelopmental disorders. J. Mol. Neurosci. 61, 590–602.
McCarthy, M., Turnbull, D.H., Walsh, C.A., Fishell, G., 2001. Telencephalic neural progenitors appear to Be restricted to regional and glial fates before the onset of neurogenesis. J. Neurosci. 21, 6772–6781.
McConnell, S.K., 1995. Constructing the cerebral cortex: neurogenesis and fate determination. Neuron 15, 761–768.
Merino, M.M., Levayer, R., Moreno, E., 2016. Survival of the fittest: essential roles of cell competition in development, aging, and cancer. Trends Cell Biol. 26 (10), 776–788.
Meyer, E.J., Ikmi, A., Gibson, M.C., 2011. Interkinetic nuclear migration is a broadly conserved feature of cell division in pseudostratified epithelia. Curr. Biol. 21, 485–491.
Micklem, H.S., Ford, C.E., Evans, E.P., Ogden, D.A., Papworth, D.S., 1972. Competitive in vivo proliferation of foetal and adult haematopoietic cells in lethally irradiated mice. J. Cell. Physiol. 79, 293–298.
Miguel-Aliaga, I., Thor, S., 2009. Programmed cell death in the nervous system-a programmed cell fate? Curr. Opin. Neurobiol. 19, 127–133.
Miyata, T., Kawaguchi, A., Okano, H., Ogawa, M., 2001. Asymmetric inheritance of radial glial fibers by cortical neurons. Neuron 31 (5), 727–741.
Moens, C.B., Prince, V.E., 2002. Constructing the hindbrain: insights from the zebrafish. Dev. Dynam. 224, 1–17.
Morata, G., Ripoll, P., 1975. Minutes: mutants of Drosophila autonomously affecting cell division rate. Dev. Biol. 42 (2), 211–221.
Moreno, E., Basler, K., 2004. dMyc transforms cells into super-competitors. Cell 117, 117–129.
Moreno, E., Basler, K., Morata, G., 2002. Cells compete for decapentaplegic survival factor to prevent apoptosis in Drosophila wing development. Nature 416, 755–759.
Namba, T., Huttner, W.B., 2017. Neural progenitor cells and their role in the development and evolutionary expansion of the neocortex, 6. Wiley Interdiscip Rev Dev Biol.
Nguyen, P.D., Gurevich, D.B., Sonntag, C., Hersey, L., Alaei, S., Nim, H.T., Siegel, A., Hall, T.E., Rossello, F.J., Boyd, S.E., Polo, J.M., Currie, P.D., 2017. Muscle stem cells undergo extensive clonal drift during tissue growth via meox1-mediated induction of G2 cell-cycle arrest. Cell Stem Cell 21, 107–119.e6.
Noctor, S.C., Flint, A.C., Weissman, T.A., Dammerman, R.S., Kriegstein, A.R., 2001. Neurons derived from radial glial cells establish radial units in neocortex. Nature 409.
Nomura, T., Ohtaka-Maruyama, C., Yamashita, W., Wakamatsu, Y., Murakami, Y., Calegari, F., Suzuki, K., Gotoh, H., Ono, K., 2016. The evolution of basal progenitors in the developing non-mammalian brain. Development 143, 66–74.
Nonaka-Kinoshita, M., Reillo, I., Artegiani, B., Ángeles Martínez-Martínez, M., Nelson, M., Borrell, V., Calegari, F., 2013. Regulation of cerebral cortex size and folding by expansion of basal progenitors. EMBO J. 32, 1817–1828.
Norden, C., Young, S., Link, B.A., Harris, W.A., 2009. Actomyosin is the main driver of interkinetic nuclear migration in the retina. Cell 138 (6), 1195–1208.
Nüsslein-Volhard, C., Gilmour, D.T., Dahm, R., 2002. Introduction:zebrafish as a system to study development and organogenesis. Zebrafish.
Oppenheim, R., 1991. Cell death during development of the nervous system. Annu. Rev. Neurosci. 14, 453–501.
Palmer, S.L., Noctor, S.C., Jablonska, B., Juliano, S.L., 2001. Laminar specific alterations of thalamocortical projections in organotypic cultures following layer 4 disruption in ferret somatosensory cortex. Eur. J. Neurosci. 13, 1559–1571.
Pan, Y.A., Freundlich, T., Weissman, T a, Schoppik, D., Wang, X.C., Zimmerman, S., Ciruna, B., Sanes, J.R., Lichtman, J.W., Schier, A.F., 2013. Zebrabow: multispectral cell labeling for cell tracing and lineage analysis in zebrafish. Development 140, 2835–2846.
Pan, Y.A., Livet, J., Sanes, J.R., Lichtman, J.W., Schier, A.F., 2011. Multicolor brainbow imaging in Zebrafish. Cold Spring Harb. Protoc. 6, 1–5.
Price, J., Thurlow, L., 1988. Cell lineage in the rat cerebral cortex: a study using retroviral-mediated gene transfer. Development 104, 473–482.
Purves, D., Lichtman, J.W., 1980. Elimination of synapses in the developing nervous system. Science 80 (210), 153–157.
Qian, X., Goderie, S.K., Shen, Q., Stern, J.H., Temple, S., 1998. Intrinsic programs of patterned cell lineages in isolated vertebrate CNS ventricular zone cells. Development 125, 3143–3152.
R Core team, 2017. R: A Lang Environ Stat Comput, R Found Stat Comput. Vienna, Austria. https://www.R-project.org.
Raff, M.C., 1992. Social controls on cell survival and cell death. Nature 356, 397–400.
Raff, M.C., 1996. Size control: the regulation of cell numbers in animal development. Cell 86, 173–175.
Reznikov, K., Acklin, S.E., Van Der Kooy, D., 1997. Clonal heterogeneity in the early embryonic rodent cortical germinal zone and the separation of subventricular from ventricular zone lineages. Dev. Dynam. 210, 328–343.
Sancho, M., Di-Gregorio, A., George, N., Pozzi, S., Sánchez, J., Pernaute, B., Rodríguez, T., 2013. Competitive interactions eliminate unfit embryonic stem cells at the onset of differentiation. Dev. Cell 26, 19–30.
Sanes, J.R., Lichtman, J.W., 1999. Development of the vertebrate neuromuscular junction. Annu. Rev. Neurosci. 22, 389–442.
Sauer, F.C., 1935. Mitosis in the neural tube. J. Comp. Neurol. 62, 377–405.
Schindelin, J., Arganda-Carreras, I., Frise, E., Kaynig, V., Longair, M., Pietzsch, T., Preibisch, S., Rueden, C., Saalfeld, S., Schmid, B., Tinevez, J.Y., White, D.J., Hartenstein, V., Eliceiri, K., Tomancak, P., Cardona, A., 2012. Fiji: an open-source platform for biological-image analysis. Nat. Methods 9 (7), 676–682.
Simpson, P., 1979. Parameters of cell competition in the compartments of the wing disc of Drosophila. Dev. Biol. 69 (1), 182–193.
Simpson, P., Morata, G., 1981. Differential mitotic rates and patterns of growth in compartments in the Drosophila wing. Dev. Biol. 85 (2), 299–308.
Smith, M.R., 2017. Ternary: an R Package for Creating Ternary Plots.
Stoner, D.S., Rinkevich, B., Weissman, I.L., 2002. Heritable germ and somatic cell lineage competitions in chimeric colonial protochordates. Proc. Natl. Acad. Sci. Unit. States Am. 96, 9148–9153.
Taghizadeh, R.R., Sherley, J.L., 2008. CFP and YFP, but not GFP, provide stable fluorescent marking of rat hepatic adult stem cells. J. Biomed. Biotechnol. 2008, 1–9.
Trevarrow, B., Marks, D.L., Kimmel, C.B., 1990. Organization of hindbrain segments in the zebrafish embryo. Neuron 4, 669–679.
van Ham, T.J., Mapes, J., Kokel, D., Peterson, R.T., 2010. Live imaging of apoptotic cells in zebrafish. FASEB J. 24 (11), 4336–4342.
Villa del Campo, C., Clavería, C., Sierra, R., Torres, M., 2014. Cell competition promotes phenotypically silent cardiomyocyte replacement in the mammalian heart. Cell Rep. 8, 1741–1751.
Walderich, B., Singh, A.P., Mahalwar, P., Nüsslein-Volhard, C., 2016. Homotypic cell competition regulates proliferation and tiling of zebrafish pigment cells during colour pattern formation. Nat. Commun. 7.
Walsh, C., Cepko, C.L., 1992. Widespread dispersion of neuronal clones across functional regions of the cerebral cortex. Science 80 (255), 434–440.
Walsh, C., Cepko, C.L., 1993. Clonal dispersion in proliferative layers of developing cerebral cortex. Nature 362, 632–635.
Weissman, I.L., 2015. Stem cells are units of natural selection for tissue formation, for germline development, and in cancer development. Proc. Natl. Acad. Sci. Unit. States Am. 112, 8922–8928.
Weissman, T.A., Pan, Y.A., 2014. Brainbow: new resources and emerging biological applications for multicolor genetic labeling and analysis. Genetics 199.
Weissman, T.A., Riquelme, P.A., Ivic, L., Flint, A.C., Kriegstein, A.R., 2004. Calcium waves propagate through radial glial cells and modulate proliferation in the developing neocortex. Neuron 43.
Woo, K., Shih, J., Fraser, S.E., 1995. Fate maps of the zebrafish embryo. Curr. Opin. Genet. Dev. 5 (4), 439–443.
Wullimann, M.F., Mueller, T., 2004. Teleostean and mammalian forebrains contrasted: evidence from genes to behavior. J. Comp. Neurol. 475, 143–162.
Yamaguchi, Y., Miura, M., 2015. Programmed cell death in neurodevelopment. Dev. Cell 32, 478–490.
Yanakieva, I., Matejčić, M., Norden, C., 2018. Choosing the right microscope to image mitosis in zebrafish embryos: a practical guide. In: Methods Cell Biol. 107–127.
Yeo, W., Gautier, J., 2004. Early neural cell death: dying to become neurons. Dev. Biol. 274, 233–244.
Yu, Y.-C., Bultje, R.S., Wang, X., Shi, S.-H., 2009. Specific synapses develop preferentially among sister excitatory neurons in the neocortex. Nature 458, 501–504.
Zhang, L.I., Tao, H.W., Holt, C.E., Harris, W.A., Poo, M.M., 1998. A critical window for cooperation and competition among developing retinotectal synapses. Nature 395 (6697), 37–44.